ORIGINAL PAPER

Impact of carbon structure and morphology on the electrochemical performance of LiFePO$_4$/C composites

**Marca M. Doeff · James D. Wilcox · Rong Yu ·
Albert Aumentado · Marek Marcinek · Robert Kostecki**

Abstract The electrochemical performance of LiFePO$_4$/C composites in lithium cells is closely correlated to pressed pellet conductivities measured by AC impedance methods. These composite conductivities are a strong function not only of the amount of carbon but of its structure and distribution. Ideally, the amount of carbon in composites should be minimal (less than about 2 wt%) so as not to decrease the energy density unduly. This is particularly important for plug-in hybrid electric vehicle applications (PHEVs) where both high power and moderate energy density are required. Optimization of the carbon structure, particularly the sp^2/sp^3 and disordered/graphene (D/G) ratios, improves the electronic conductivity while minimizing the carbon amount. Manipulation of the carbon structure can be achieved via the use of synthetic additives including iron-containing graphitization catalysts. Additionally, combustion synthesis techniques allow co-synthesis of LiFePO$_4$ and carbon fibers or nanotubes, which can act as "nanowires" for the conduction of current during cell operation.

M. M. Doeff (✉) · J. D. Wilcox · R. Yu · A. Aumentado
Materials Sciences Division,
Lawrence Berkeley National Laboratory,
University of California,
Berkeley, CA 94720, USA
e-mail: mmdoeff@lbl.gov

M. Marcinek · R. Kostecki
Environmental Energy Technologies Division,
Lawrence Berkeley National Laboratory, University of California,
Berkeley, CA 94720, USA

Introduction

LiFePO$_4$ is a technologically important material currently of interest as a cathode for lithium ion batteries. The relatively high theoretical capacity of 170 mAh/g delivered at moderate potentials (~3.45 V vs Li) and tolerance against thermal abuse and overcharge make it particularly attractive for vehicular applications, where safety is a paramount concern. In its native state, LiFePO$_4$ has low electronic conductivity (10^{-9} S/cm) [1, 2], which limits the rate capability in lithium cells. In early reports [3], full utilization was not achieved even at low current densities. The rate problem has been ameliorated by carbon-coating LiFePO$_4$ particles during synthesis [4] and/or minimizing primary particle size [5]. However, even relatively small amounts of added carbon adversely affect energy density [6]. Devices designed for use in plug-in hybrid electric vehicles (PHEVs) require both high power and moderate energy densities, requiring that LiFePO$_4$ cathode materials be carefully optimized. The bricklayer model [7] predicts that, under ideal circumstances, it is more effective to increase the electronic conductivity of the grain boundary phase than to increase its quantity to maximize the pressed pellet composite conductivities. This indicates that it should be fruitful to direct effort toward improving the conductivity of surface carbon in composites so as to minimize the amount required, provided that these composite conductivities accurately reflect the electrochemical performance in lithium cells.

Recent work in our laboratory has been directed towards the optimization of the structure of carbon in LiFePO$_4$/C composites intended for use in battery applications [8].

Because the structure (in particular, sp^2/sp^3 and disordered/graphene (D/G) ratios) closely correlates with electronic conductivity, this allows minimization of the carbon content in the composites. Strategies to improve structure include the use of synthetic additives such as graphitization catalysts, incorporated before the final calcination process. Alternatively, combustion techniques allow carbon to be produced rapidly at temperatures normally above the stability limit of LiFePO$_4$. The combustion product can then be calcined at lower temperatures to form carbon-coated LiFePO$_4$. Under certain conditions, carbon nanotubes or fibers are produced during this process. These can act as conductive "nanowires" for the passage of current.

Materials and methods

LiFePO$_4$/C composites were prepared either by a previously described sol-gel method [9] or by combustion synthesis using citric acid [10], glycine [11], or urea [12] and metal nitrate and dihydrogen ammonium phosphate precursors. Products from the latter process were then calcined at 600 °C under an atmosphere of flowing 5% H$_2$ in N$_2$ in a quartz tube furnace for 4 h. Pyromellitic acid and graphitization catalysts (iron nitrate or ferrocene) were optionally added before the final calcination step in the case of the sol-gel synthesis. For comparison purposes, carbon from pure ferrocene or ferrocene/pyromellitic acid mixtures was produced by placing the precursors in copper foil packets sealed into quartz tubes and heating at 700 °C for 1 h.

LiFePO$_4$ phase purity was assessed by powder X-ray diffraction (XRD) using a Philips X'Pert diffractometer (θ–θ geometry, back monochromator) equipped with an X'Celerator detector, using Cu K-alpha radiation. Luvak, Boylston, MA performed carbon and hydrogen analyses, used to determine H/C ratios, on selected samples. Images were obtained with a Hitachi S-4300SE/N scanning electron microscope (SEM) or a JEOL-7500C SEM equipped with a scanning transmission electron microscopy (STEM) detector. The transmission electron microscopy (TEM) study was performed using a Phillips CM200 microscope operated at an accelerating voltage of 200 kV with a field emission gun. The electron energy loss spectra (EELS) were collected with a Gatan Imaging Filter system attached to the microscope.

Raman spectra were obtained on composite powders or carbon products from the ferrocene and pyromellitic acid pyrolyses using an integrated confocal Raman microscope system, "Labram," made by ISA Group Horiba, as previously described [8]. Pressed pellets for conductivity studies were fabricated by uni-axially pressing ~0.5 g of active material to 10 kpsi in a 1/2″ stainless steel die. The pellets were then transferred into balloon holders and cold isostatically pressed to 180 kpsi achieving a final density of ~70% of the theoretical LiFePO$_4$ density (3.6 g/cm^3). Thin gold electrodes were then sputtered on to each face of the pellet using a Bal-Tec SCD 050 sputter coater. AC impedance spectra were obtained using a Solartron Instruments 1260 impedance/gain-phase analyzer at selected temperatures between 25 and 200 °C. Conductivities were derived from the intercepts of the capacitative arcs with the z'-axes in the Nyquist plots.

Electrodes were composed of 80 wt% active material, 8 wt% Kynar poly(vinylidene fluoride) (Elf Atochem North America, Technical Polymers Department), 6 wt% SFG-6 synthetic flake graphite (Timcal, Graphites and Technologies), and 6 wt% acetylene black. Electrodes were cast as a slurry in 1-methyl-2-pyrrolidinone (Sigma Aldrich, 99%) onto carbon-coated aluminum current collectors (Intelicoat Technologies) and dried for 24 h in air followed by 12–24 h in a vacuum oven at 120 °C. Cathodes with an area of 1.8 cm^2 were punched from the cast electrode and typically had loadings of about 1 mAh/cm^2. Assembly of lithium half-cells in 2,032 coin cells was performed in a helium-filled glove box using 1 M LiPF$_6$ in 1:2 ethylene carbonate/dimethylcarbonate electrolyte solution and a Celgard 3401 separator. At least two cells of the same type were tested for each material to ensure reproducibility. Electrochemical studies were undertaken galvanostatically using an Arbin BT/HSP-2043 and/or a Macpile II (Bio-Logic, S.A., Claix, France) automated cycling data recorder between 2.0 and 3.9 V at room temperature. Cells were always charged at a current density corresponding to C/25 and allowed to rest 15 min between half-cycles.

Results and discussion

The strong correlation between the rate capability of LiFePO$_4$/C composites in lithium half-cells and the room-temperature-pressed pellet conductivities is clearly shown in Fig. 1. It is significant that conductivities and rate capabilities do not always track carbon content; for example, compare the two 0.71% C samples in the graph. The differences between the two materials reflect the increase in the carbon sp^2/sp^3 ratio that occurs when an iron nitrate graphitization catalyst is used in addition to pyromellitic acid during the final calcination step [8].

It is common for laboratory samples of LiFePO$_4$, particularly those made from precursors with organic moieties (oxalates, acetates, etc.), to contain some carbon, the amount of which depends upon furnace conditions. The quality of this carbon, as determined by Raman microprobe spectroscopy, varies [13] most likely as a result of small differences in iron oxide contents and other surface impurities. Both the in situ carbon content and its structure may be reliably manipulated via the use of synthetic
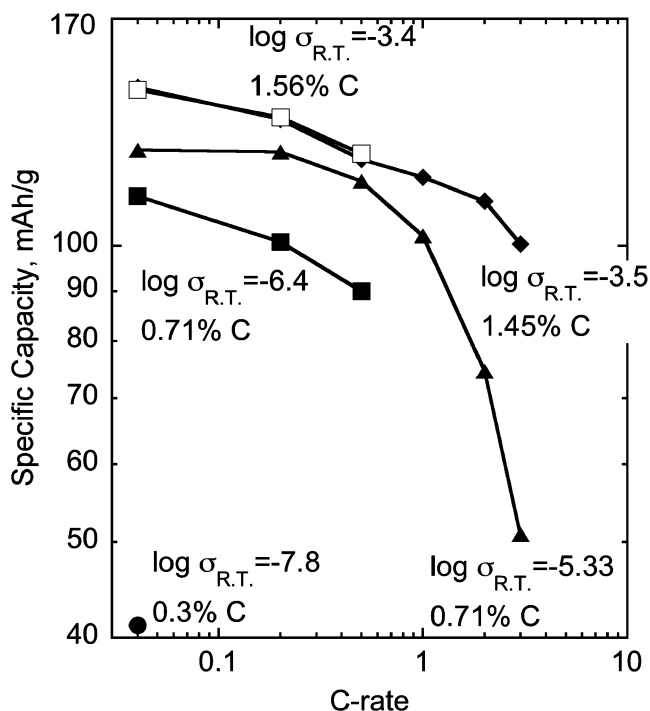
Fig. 1 Peukert plot showing the rate capabilities of lithium cells with LiFePO$_4$/C composites. The room-temperature-pressed pellet conductivities and in situ carbon contents of the composites are marked on the graph (note that the latter does not include the carbon added to the electrode, which was the same for all examples)

additives. These must, however, be carefully chosen. Polyaromatic compounds or polymers with low H/C ratios are sometimes used to produce conductive carbons at temperatures above 1,000 °C [14–16] but may not decompose completely at the low synthesis temperatures (<750 °C) at which LiFePO$_4$ is produced. The carbon content in these samples is increased over materials processed without the additives, but electrochemical performance is poor, presumably because of the rather low electronic conductivities of the incompletely decomposed coatings [9]. In contrast, the addition of the somewhat volatile pyromellitic acid (1,2,4,5-benzenetetracarboxylic acid) during synthesis of LiFePO$_4$ only slightly increases carbon contents but improves both the composite conductivities and the electrochemical performance of these electrode materials in lithium cells. This is directly attributable to the increased graphene content of the in situ carbon (i.e., higher sp^2/sp^3 and lower D/G ratios) as determined by analysis and deconvolution of Raman data obtained on the powders [8].

Further improvements can be realized by the addition of very small amounts of iron containing graphitization catalysts, such as iron nitrate, with the pyromellitic acid during synthesis. This does not change the amount of in situ carbon but increases its sp^2/sp^3 ratio (graphene content), which results in improved composite conductivity and electrochem-

ical performance such as that seen in Fig. 1. In contrast, samples produced with both pyromellitic acid and ferrocene or ferrocenecarboxylic acid have higher carbon contents than those made with pyromellitic acid alone, although the structure is, somewhat surprisingly, unchanged. The increased composite conductivity and better electrochemical performance (see samples with 1.45 and 1.56% carbon in Fig. 1) are due mainly to the differences in the carbon amounts. It is interesting to note that using ferrocene alone as a synthetic additive results in composites with very low carbon contents and poor performance. Both pyromellitic acid and ferrocene are volatile and tend to sublime during calcination. While this results in some loss of carbon during synthesis, it improves the homogeneity of the coatings and results in a more even distribution of the coating over the somewhat porous and agglomerated particles [17].

These coatings adhere very well and are able to withstand more than 100 deep discharge cycles without significant degradation [18].

Some LiFePO$_4$/C samples processed with small amounts of ferrocene and pyromellitic acid showed somewhat better electrochemical performance than expected based on the low carbon contents. These powders exhibited additional peaks at low wave numbers in the Raman spectra in some spots, which could be attributed to the presence of inhomogeneously distributed Fe$_3$C on the surfaces of the powders. Because peaks from Fe$_3$C interfere with those attributable to carbon, it is not possible to determine the structure of the latter in these samples. However, the pyrolysis of ferrocene or ferrocene and pyromellitic acid in the absence of LiFePO$_4$ or LiFePO$_4$ precursors provides some insights as to the nature of the carbon in the aforementioned samples. Figures 2 and 3 show SEM images and the accompanying Raman spectra taken on the products of the ferrocene and pyromellitic acid thermal decomposition.

The carbon produced by pyrolyzing mixtures of ferrocene and pyromellitic acid alone exhibits an interesting and unique star-like morphology (Fig. 2). The arms of the stars are as long as 2 μm, and some encase narrower scroll-like structures (see, for example, the upper left arm of the center star in the SEM image in Fig. 2). The Raman spectra obtained on several spots of the samples containing stars are typical of disordered carbons (Fig. 2, graph on right). The two most prominent peaks, at 1,324 and 1,590 cm^{-1} correspond to the E_{2g} and A_{1g} vibration modes or the so-called D (disordered) and G (graphene) bands of sp^2-type carbon, respectively. The origin of the D-band is associated with the breakage of symmetry that occurs at the edges of graphite sheets and point defects, so that the D/G peak intensity ratio can be used as rough measure of the graphene domain size [19]. Two other less prominent peaks, centered near 1,190 and 1,518 cm^{-1}, are commonly assigned to vibrational modes of sp^3-type carbon. Decon-

Fig. 2 SEM image of carbon stars obtained via combustion of a 1:1 mixture of ferrocene and pyromellitic acid at 700 °C (*left*) and Raman spectra obtained at three different spots on the product (*right*). The D (disordered) and G (graphene) bands attributable to carbon are marked
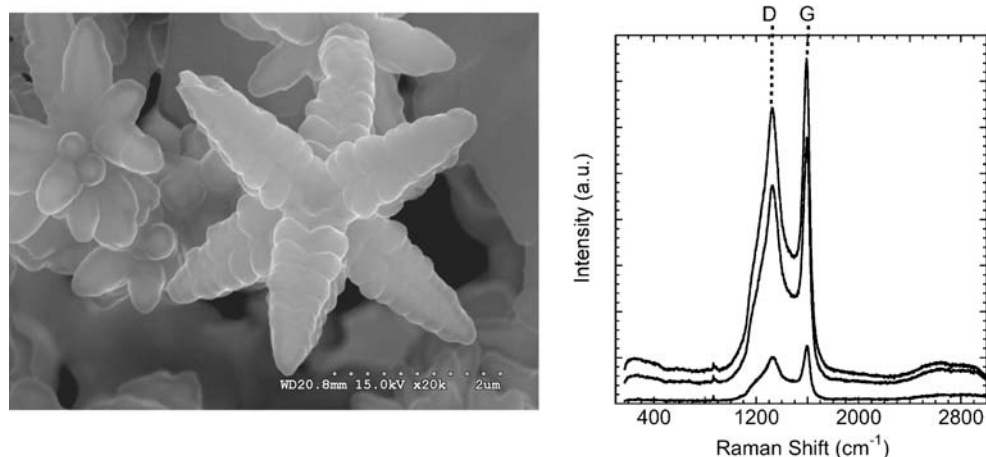

volution of these peaks yields the sp^2/sp^3 ratios that correlate to conductivity. Alternatively, the depth of the saddle between the D and G peaks and their relative peak intensities can be used as a qualitative indicator of the carbon structure. At any rate, the carbon region of the Raman spectra obtained on most samples of $LiFePO_4$ processed with ferrocene and pyromellitic acid resembles that presented in Fig. 2.

Pyrolysis of ferrocene alone results in the production of extremely small particles and nanotubes less than 10 nm in diameter (Fig. 3, left). The Raman spectra vary from spot to spot in the sample (Fig. 3, right). Peaks at low wave numbers in the upper spectrum shown in the graph in Fig. 3 are identical to those found in the anomalous ferrocene and pyromellitic acid treated $LiFePO_4$ samples and can be likewise assigned to Fe_3C (note that the relative peak heights of the D and G bands in the upper spectrum differ from those of the lower one, illustrating the effect of the presence of Fe_3C on the carbon bands).

Iron or iron carbide nano-particles act as nucleation sites for the growth of carbon nanotubes [20] under conditions similar to those used in this study and for the synthesis of $LiFePO_4$. Carbon nanotubes resulting from the pyrolysis of ferrocene or ferrocene/hydrocarbon mixtures and subsequent formation of Fe_3C have been observed in previous studies [21, 22]. The geometries, types [e.g., single-walled (SWCNT) or multi-walled (MWCNT)] and relative amounts of nanotubes vs other types of carbon formed are complex functions of the iron/carbon ratio in the feedstock and other synthesis conditions [23, 24].

The vibrational spectroscopy of carbon nanotubes as a function of their structure (diameter, helicity, etc.) has been described in the literature [25, 26]. Unfortunately, interference from other types of carbon and iron carbide in the samples in this study makes it impossible to detect the presence of nanotubes or identify their structures by Raman spectroscopic means. At present, their presence can only be identified using microscopy or inferred from

Fig. 3 SEM image of carbon nanotubes and carbon and Fe_3C particles obtained via combustion of ferrocene alone at 700 °C (*left*) and Raman spectra obtained at two different spots on the products. Peaks at low wave numbers in the upper spectrum are attributable to Fe_3C. The D (disordered) and G (graphene) bands attributable to carbon are marked; however, Fe_3C bands in the upper spectrum interfere with these
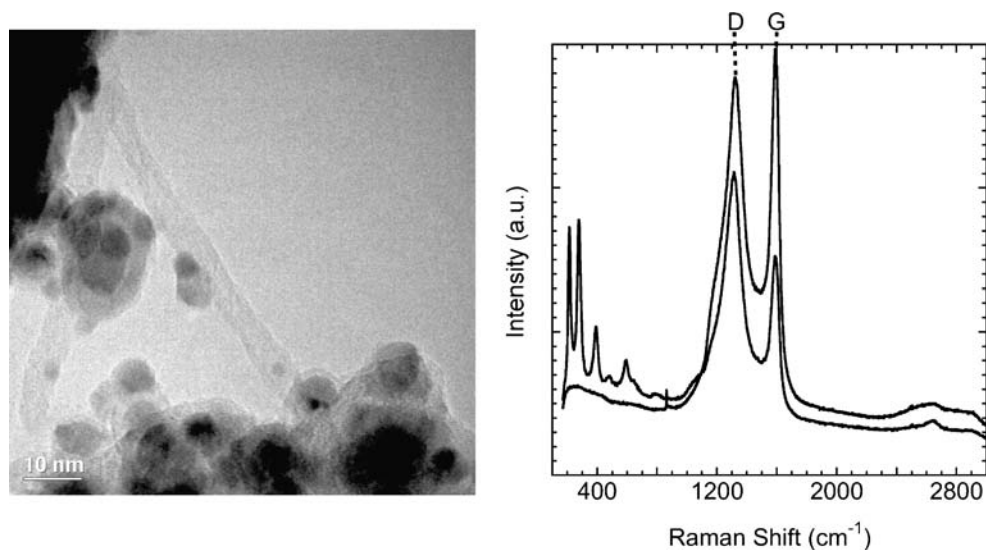
the observation of Fe₃C in the Raman spectra of the composite powders.

The possibility of forming carbon nanotubes under the same conditions as those used for making LiFePO₄/C composites is significant. Depending upon structure (diameter, helicity, and the presence or absence of defects), carbon nanotubes are metallic or semi-conducting. Their high aspect ratios mean that, in principle, very low volume fractions are needed to achieve percolating thresholds; e.g., percolation for electronic conductivity was achieved using only 0.1 vol% SWNTs in epoxy in one report [27]. This suggests that both the coating amounts on powders and the added carbon in the composite electrodes could be substantially reduced if carbon nanotubes are produced during LiFePO₄ synthesis. Co-synthesis has cost, fabrication, and safety advantages over mixing in nanotubes during the electrode manufacturing process; therefore, this is an attractive prospect for maximizing power capability while simultaneously minimizing carbon contents.

The low temperature at which LiFePO₄ is normally calcined during traditional solid state or sol-gel methods (typically below 700–750 °C), however, limits the extent to which the conductivity of carbon coatings can be improved. In contrast, combustion synthesis techniques allow the carbon and LiFePO₄ production to be formed in separate steps and at different temperatures. For these methods, metal nitrate precursors are typically dissolved in water in the desired ratios, and a complexing agent/fuel such as glycine, citric acid, or urea is added. The solution is then boiled to dryness, at which point spontaneous combustion occurs. The type of fuel and the nitrate/fuel ratio determine the temperature at which this occurs and can reach as high as 1,450 °C [11]. The product of the initial combustion is carbon and a precursor to LiFePO₄, which is subsequently formed during a brief calcination at 600 °C under N₂/H₂. The type and amount of fuel determine the final carbon content in the composite. The addition of pyromellitic acid to solution before combustion boosts the carbon content under conditions where little or no carbonaceous residue is produced (e.g., when glycine is used). Although the phase purity of the final products is sensitive to the exact ratios of the precursors used and the conditions of combustion, with a little effort, materials with no iron oxide impurities (as determined by XRD analyses) can be produced by this method.

The improvement in the carbon structure for combusted LiFePO₄/C composites is evident when the Raman spectra on these powders are compared to the samples made by sol-gel processing, even for those processed with graphitization catalysts (Fig. 4). The G-band is sharper and the saddle point between the D and G bands deeper, suggesting a higher sp^2/sp^3 ratio than that found for the sol-gel materials processed with pyromellitic acid and either ferrocene or iron nitrate.
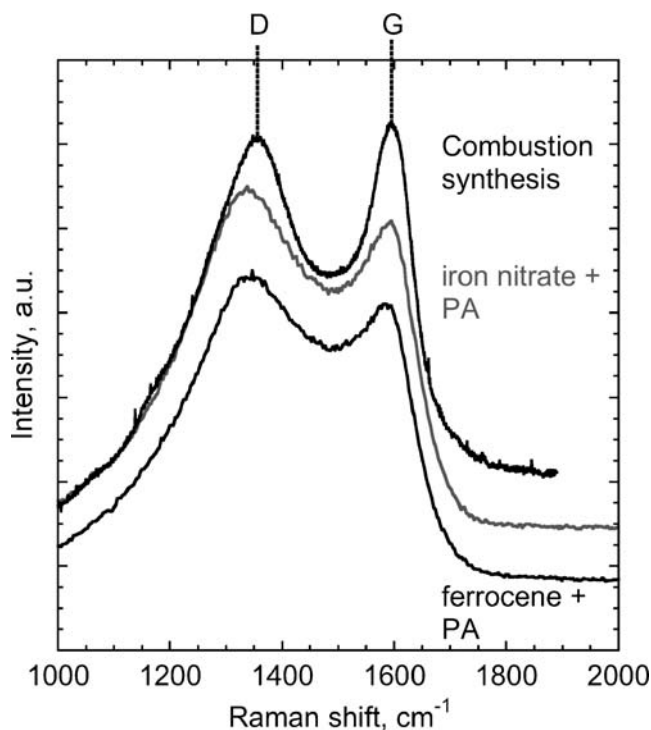

Fig. 4 The carbon region of Raman spectra taken on LiFePO₄/C composites produced by combustion synthesis (*top*), sol-gel processing with pyromellitic acid (*PA*) and iron nitrate added before the final calcination (*middle*) and sol-gel with ferrocene and pyromellitic acid (*bottom*). The D and G bands of carbon are marked

Interestingly, some samples prepared by combustion synthesis contained copious quantities of long fibers (Fig. 5), approximately 30 nm in diameter. Both the high-resolution image (bottom left) and the energy loss near edge spectrum show that these fibers are composed of amorphous carbon. In other preparations, several types of carbon nanotubes can be readily detected (Fig. 6).

Which exact synthetic parameters are responsible for the formation of carbon nanotubes vs solid fibers during combustion are not presently known. However, the bottom right image in Fig. 6, which clearly shows an entire isolated carbon nanotube, may provide some clues. The upper portion of the nanotube is closed off at the end and contains a high-z material (i.e., one containing iron). The bottom portion of the tube is hollow, except for an iron-containing nanoparticle. During combustion of an iron-containing catalyst and a carbon source, carbon nanotubes nucleate at the sites of catalytic nanoparticles made up of iron oxide or iron carbide [28]. The geometry of the nanotube is determined by the conditions and the hydrocarbon source; it is interesting to note that the use of benzene as a feedstock results in highly defective, kinked, metal-filled MWCNTs such as those seen in Fig. 6, whereas SWCNTs are produced from more readily decomposed acetylene or ethylene [29]. Solid filaments such as those seen in Fig. 5 are produced under similar conditions as nanotubes but

Fig. 5 TEM images of fibers found in a LiFePO$_4$/C composite synthesized by combustion synthesis (*top and bottom left*). EELS analysis (*bottom right*) shows that these fibers consist of amorphous carbon
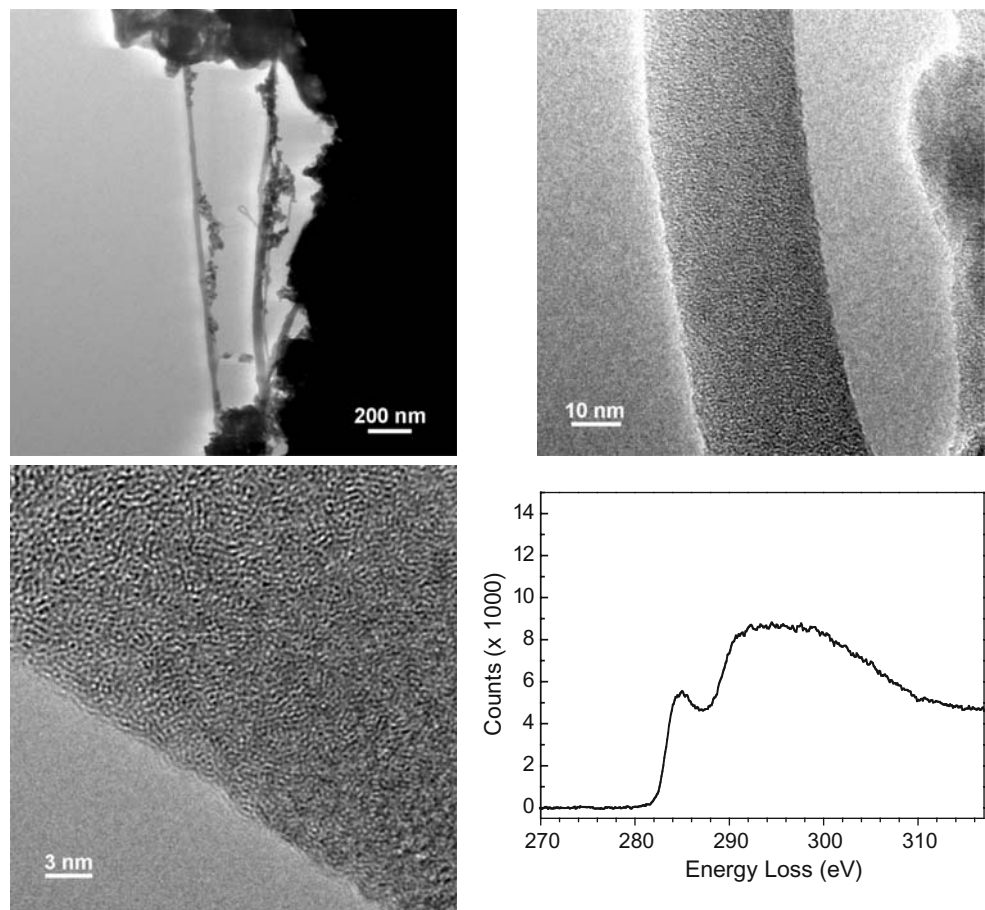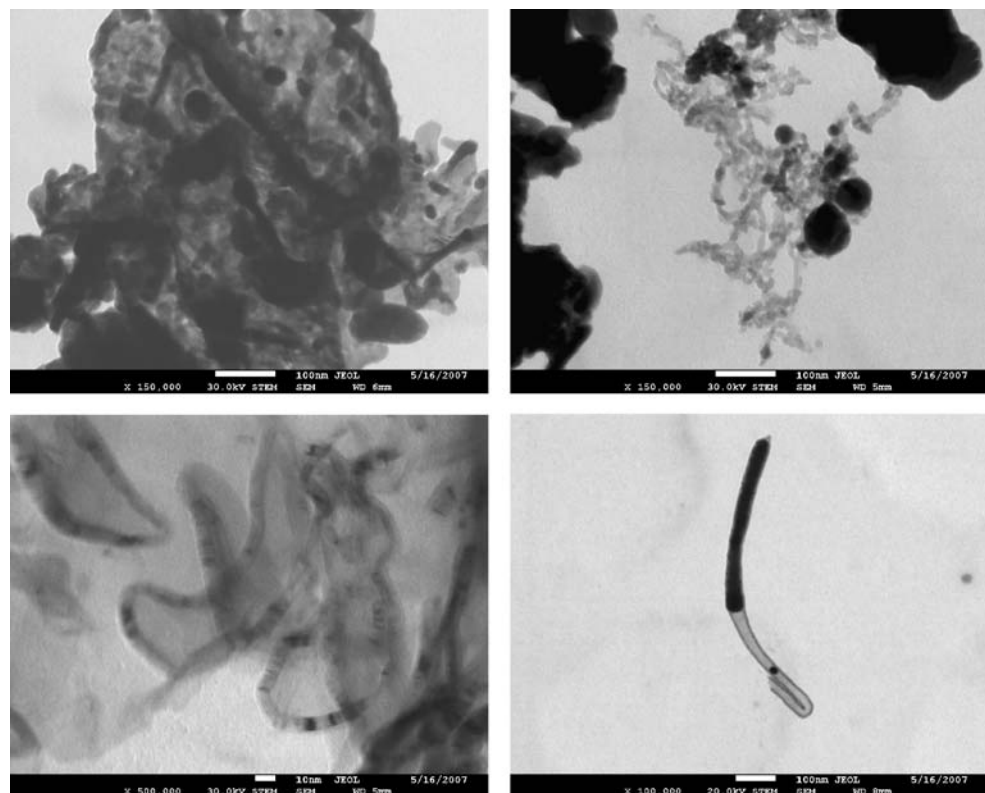

Fig. 6 SEM/STEM images of a LiFePO$_4$/C composite showing carbon nanotubes. *Dark areas* correspond to high-z materials (e.g., LiFePO$_4$) and *lighter gray areas* to low-z materials (carbon)

nucleate from larger catalyst particles. This suggests that the presence of trace amounts of iron oxide produced during combustion of aqueous mixtures of iron nitrate catalyze the formation of carbon fibers or nanotubes in the $LiFePO_4$/C composites discussed in this paper. Therefore, the geometries of the nanotubes should be possible to control through judicious choice of a hydrocarbon source. For example, it appears that pyromellitic acid plays a similar role to that of benzene in the combustion studies described in references [28] and [29] in causing the formation of defective MWCNTs rather than SWCNTs. The presence of defects, such as kinks, adversely affects electronic conductivity, suggesting that a more readily decomposed non-aromatic hydrocarbon source may be preferable to pyromellitic acid.

Further work in this laboratory will be directed towards optimization of the synthetic parameters needed to produce lithium metal phosphate/carbon nanotube and carbon fiber composites and characterization of these materials.

Conclusions

The impact of the carbon structure on the electrochemical performance of $LiFePO_4$/C composites has been presented. Carbon coatings with more graphitic character (e.g., sp^2/sp^3 ratios) result in higher composite conductivities, which correlate well with rate capabilities in electrochemical cells. While the carbon structure can be manipulated to some extent via the use of organic precursors and graphitization catalysts added before calcination, the low temperature at which $LiFePO_4$ is typically synthesized presents limitations. Combustion synthesis, where a high temperature combustion step is followed by a brief calcination at lower temperatures, allows the formation of carbon to be decoupled from $LiFePO_4$ production. Under certain conditions, carbon fibers or nanotubes are formed.

References

1. Chung SY, Bloking JT, Chiang YM (2002) Nat Mater 1:123
2. Shi S, Liu L, Ouyang C, Wang DS, Wang Z, Chen L, Huang X (2003) Phys Rev B 68:195108
3. Padhi AK, Nanjundaswamy KS, Goodenough JB (1997) J Electrochem Soc 144:1189
4. Ravet N, Goodenough JB, Besner S, Gauthier M, Armand M (1999) The Electrochemical Society and the Electrochemical Society of Japan Meeting Abstracts, vol. 99–2, abstract 127, Honolulu, HI
5. Delacourt C, Poizot P, Levasseur S, Masquelier C (2006) Electrochem Solid State Lett 9:A352
6. Chen Z, Dahn JR (2002) J Electrochem Soc 149:A1184
7. Maier J (2003) Solid State Ionics 157:327
8. Wilcox JD, Doeff MM, Marcinek M, Kostecki R (2007) J Electrochem Soc 154:A389
9. Hu Y, Doeff MM, Kostecki R, Fiñones R (2004) J Electrochem Soc 151:A1279
10. Zhang J, Gao L (2004) Mat Res Bull 39:2249
11. Chick LA, Pederson LR, Maupin GD, Bates JL, Thomas LE, Exarhos GJ (1990) Mater Lett 10:6
12. Junior AF, de Oliveira Lima EC, Novak MA, Wells PR (2007) J Magn Magn Mater 308:198
13. Doeff MM, Hu Y, McLarnon F, Kostecki R (2003) Electrochem Solid State Lett 6:A207
14. Renschler CL, Sylwester AP, Salgado LV (1989) J Mater Res 4:452
15. McKeown NB (2000) J Mater Chem 10:1979
16. Kamiya K, Noda T, Ide M, Tanaka J (1995) Synth Met 71:1765
17. Gabrisch H, Wilcox JD, Doeff MM (2006) Electrochem Solid State Lett 9:A360
18. Gabrisch H, Doeff MM, Wilcox J (2006) 2006 Joint International Meeting of the Electrochemical Society (ECS) and Sociedad Iberoamericana de Electroquimica, vol. 2006-2, abstract 177. Cancun, Mexico
19. Tuinstra F, Koenig J (1970) Chem Phys 53:1126
20. Emmenegger C, Bonard JM, Mauron P, Sudan P, Lepora A, Grobety B, Zuttel A, Schlapbach L (2003) Carbon 41:539
21. Rao CNR, Sen R, Satishkumar BC, Govindaraj A (1998) Chem Commun 1525
22. Andrews R, Jacques D, Rao AM, Derbyshire F, Qian D, Fan X, Dickey EC, Chen J (1999) Chem Phys Lett 303:467
23. Vander Wal R, Hall LJ (2002) Combust Flame 130:27
24. Hou H, Schaper AK, Weller F, Greiner A (2002) Chem Mater 14:3990
25. Eklund PC, Holden JM, Jishi RA (1995) Carbon 7:959
26. Rao AM, Richter E, Bandow S, Chase B, Eklund PC, Williams KA, Fang S, Subbaswamy KR, Menon M, Thess A, Smalley RE, Dresselhaus G, Dresselhaus MS (1997) Science 275:187
27. Biercuk MJ, Llaguno MC, Radosavljevic M, Hyun JK, Johnson AT, Fischer JE (2002) Appl Phys Lett 80:2767
28. Height MJ, Howard JB, Tester JW, Vander Sande JB (2004) Carbon 42:2295
29. Diener MD, Nichelson N, Alford JM (2000) J Chem Phys B 104:9615